Results in Applied Mathematics 28 (2025) 100641

Contents lists available at ScienceDirect

Results in Applied Mathematics

journal homepage: www.elsevier.com/locate/results-in-applied-mathematics

Mathematical analysis of shallow water wave and the generalized Hirota-Satsuma-Ito models: Soliton solutions and their interactions

M. Belal Hossen [a,*], Md. Towhiduzzaman [a], Harun-Or-Roshid [b,c], K. M. Abdul A. Woadud [a]

[a] Department of Mathematics, Uttara University, Bangladesh
[b] Department of Mathematics, Pabna University of Science and Technology, Bangladesh
[c] Department of Mathematics, Sunamgonj Science and Technology University, Bangladesh

ARTICLE INFO

Keywords:
Shallow water wave equation
gHSI
Soliton
Rogue wave
Solitary wave
Lump wave

ABSTRACT

This study investigates the mathematical properties and soliton dynamics of the (2+1)-dimensional extended Shallow Water Wave (eSWW) and the generalized Hirota-Satsuma-Ito (gHSI) models by Hirota bilinear scheme. A comprehensive mathematical analysis is conducted to derive multi-soliton solutions, including 2-soliton and 3-soliton solutions, while breather, rogue and lump solutions derive from 2-soliton. Investigation focuses on soliton interactions under various conditions, with particular attention to special cases like rogue and lump type solutions, highlighting their distinct characteristics and physical significance. Additionally, the analysis extends to the gHSI equation, where long wave limit scheme is applied to attain rogue and lump wave solutions. We analyzed the planar dynamics of the system to assess its sensitivity. These findings enhance our knowledge of nonlinear wave processes, with potential applications in oceanography, fluid mechanics, and related scientific fields.

1. Introduction

The study of precise solutions and innovative structures in nonlinear partial evolution models (NLPEMs) is a significant area of research within soliton theory. In recent years, considerable efforts have been dedicated to exploring solitonic solutions and various interaction types in NLPEMs. These investigations employ a variety of analytical methods, including the inverse scattering transform [1], (G'/G)-expansion scheme [2], Riemann–Hilbert (RH) approach [3], homogeneous balance approach [4], Hirota's bilinear approach [5–10], sub-equation method [11], MSE method [12], trial function technique [13], and bilinear network approach [14]. Among these methods, Hirota's bilinear approach has proven to be particularly effective in deriving exact solitonic solutions for NLPEMs. Once the bilinear form of an NLPEM is determined, it enables the construction of rogue waves, multi-soliton solutions, and breather waves.

In recent decades, researchers have become increasingly interested in dynamic solutions, particularly lump-rogue solutions, which transpire in various physical phenomena like deep ocean waves, Bose–Einstein condensates, and nonlinear optics. Lump solutions are analytical rational-function solutions that remain localized within a small region along all spatial directions, whereas lump waves are

* Corresponding author.
E-mail address: belalshimul14@gmail.com (M.B. Hossen).

https://doi.org/10.1016/j.rinam.2025.100641
Received 19 May 2025; Received in revised form 5 September 2025; Accepted 12 September 2025
Available online 19 September 2025

similarly localized but may not occupy every spatial path [15–17]. In contrast, rogue waves are exceptionally large, unpredictable, and transient surface waves that can pose serious hazards to ships in deep oceans, occasionally causing capsizing due to their extreme amplitude. Rogue waves are localized both in space and time, appear suddenly, and disappear without leaving a trace [18,19], making them responsible for numerous oceanic disasters. Special lumps may produce in considering the long-wave limits of N-soliton solutions [20]. Many integrable equations exhibit a remarkable variety of lump solutions, including the KPI model [21], DJKM model [22], Soliton model [23], BKP model [24,25], Camassa–Holm–KP model [26], Ishimori-I model [27], and KP model from a self-sufficient source [28]. It is common to refer to rogue waves as "freak waves". Recent studies have extensively examined the interactions of solitons, lumps, rogue waves, and hybrid solutions in various nonlinear models [29–31].

In the present work, we generalise the ansatz equation in the bilinear technique to get travelling waves for the extended (2+1)-dimensional SWW model [32] and (2+1)-dimensional gHSI model [33]. As a result, we derive novel and more complete exact solutions for travelling waves. The following are the governing models:

$$u_{yt} + 3u_{xxxy} - 3u_{xx}u_y - 3u_xu_{xy} + \eta u_{xy} = 0 \tag{1}$$

$$u_{xxxt} + 3(u_xu_t)_x + u_{yt} + u_{xx} - u_{xy} + u_{xt} - u_{yy} = 0 \tag{2}$$

whereη is a constant. Karunakar and Chakraverty [34] employed the Homotopy Perturbation Technique on derive solutions for the (1+1)-D SWW models, demonstrating its effectiveness in handling nonlinearities inherent in such models. Zahran and Khater [35] applied this technique to construct solutions expressible in terms of Jacobian elliptic functions, providing insights into the wave behaviors described by SWW equations. Liu et al. [36] proposed a combination of the homotopy perturbation scheme and the Mohand transform for addressing two-dimensional linear and nonlinear SWW equations, offering approximate solutions and graphical insights into water surface elevation variations over time and depth. Wei and Cai [37] used the generalized bilinear technique to derive accurate rational solutions for a SWW-like equation, expanding the set of acknowledged solutions and providing a framework for exploring more complex wave interactions. Roshid et al. [32] discuss the dynamics the lump and solitary wave, whereas in this work we discussed multi-wave solutions such as two solitons, three solitons, breather wave, rogue wave and lump wave solutions with 3-D and contour plot. Ma et al. [33] utilized the Hirota's technique to originate lump waves for a (2+1)-dimensional gHSI model. Xiao et al. [38] investigated the gHSI model utilising the three-wave process associated with the bilinear form. Fan et al. [39] executed the semi-inverse variational algorithm to the (2+1)-dimensional gHSI model, obtaining rational function solutions and exploring periodic and cross-kink wave solutions, providing a broader perspective on the equation's solution space. Guo et al. [40] employed the multiple rogue waves derived from Hirota's bilinear technique to construct various soliton wave solutions for gHSI model whereas in this work we discussed multi-wave solutions such as two solitons, three solitons, breather wave, also using long-wave limit approach we discuss lump wave and rogue wave solutions of gHSI equation with 3-D and contour plot. This study conducts a comprehensive mathematical analysis to derive multi-wave solutions, including two-wave and three-wave, breather wave and lump wave solutions. Additionally, the analysis extends to the gHSI equation, where the long-wave limit scheme is applied for achieving lump and rogue wave solutions.

The manuscript is laid out this way: Section 2 presents the mathematical analysis of the extended (2+1)-dimensional SWW model. Section 3 explores the multi-wave solutions of the SWW model. Section 4 examines the mathematical analysis of the (2+1)-dimensional gHSI model. Section 5 discusses multi-wave solutions of gHSI model. Section 6 presents the sensitivity analysis of the proposed nonlinear problem. Section 7 offers a comparison with published results with novelties. Finally, Section 8 offers a summary and concluding remarks.

2. Mathematical analysis of the shallow water wave model

The initial step in solving Eq. (1) involves re-expressing the equation below Hirota's bilinear form

$$\left(D_yD_t + D_x^3D_y + \eta D_xD_y\right)\Theta\cdot\Theta - \alpha\Theta^2 = 0, \tag{3}$$

wherein the bilinear operator shown below is used.

$$D_x^{\alpha}D_y^{\beta}D_t^{\gamma}(\Theta\cdot\Phi) = \left(\frac{\partial}{\partial x} - \frac{\partial}{\partial x'}\right)^{\alpha}\left(\frac{\partial}{\partial y} - \frac{\partial}{\partial y'}\right)^{\beta}\left(\frac{\partial}{\partial t} - \frac{\partial}{\partial t'}\right)^{\gamma} \times \Theta(x,y,t)\cdot\Phi(x',y',t')|_{x=x',y=y',t=t'} \tag{4}$$

Let's now implement the function conversion that follows.

$$u = -2(\ln\Theta)_x = -2\frac{\Theta_x}{\Theta}. \tag{5}$$

Applying the following operator defined in Eq. (4) to the components of Eq. (3) results in

$$\begin{aligned}
&\left(D_x^3D_y\right)\Theta\cdot\Theta = 2\Theta\Theta_{3xy} - 6\Theta_{2xy}\Theta_x + 6\Theta_{xy}\Theta_{2x} - 2\Theta_{3x}\Theta_y \\
&\left(D_yD_t\right)\Theta\cdot\Theta = 2\Theta\Theta_{yt} - 2\Theta_y\Theta_t \\
&\left(D_xD_y\right)\Theta\cdot\Theta = 2\Theta\Theta_{xy} - 2\Theta_x\Theta_y
\end{aligned} \tag{6}$$

Thus, by considering the bilinear differential operator (6) for Eq. (1) and applying the transformation (5), we derive

$$2\left(\Theta\Theta_{3xy} - 3\Theta_{2xy}\Theta_x + 3\Theta_{xy}\Theta_{2x} - \Theta_{3x}\Theta_y + \Theta\Theta_{yt} - \Theta_y\Theta_t\right) + 2\eta\left(\Theta\Theta_{xy} - \Theta_x\Theta_y\right) - \gamma\Theta^2 = 0 \tag{7}$$

In this article, we will keep trying to construct our analytical solutions mostly based on Eq. (7).

3. Multi-wave solutions of SWW model

Normally, Hirota's bilinear approach [39] is employed to generate soliton solutions. Assume that displays multi-solitons in a way stated below:

$$f = f_M = \sum_{\varepsilon=0,1} \exp\left(\sum_{i=1}^{M} \mathrm{X}_i\vartheta_i + \sum_{i<j}^{M} \mathrm{X}_i\mathrm{X}_j C_{ij}\right) \tag{8}$$

3.1. The 2-soliton solutions and their modified structures

We set$M = 2$, thenf_2 obtained as

$$f_2 = 1 + \exp\vartheta_1 + \exp\vartheta_2 + C_{12}\exp(\vartheta_1 + \vartheta_2), \tag{9}$$

where,

$$\vartheta_i = k_i(x + p_i y + q_i t) + \vartheta_i^0, \tag{10}$$

By substituting (9) into (3) and simplifying, setting exponential terms' coefficients to all equal zero, that leads to the ensuing

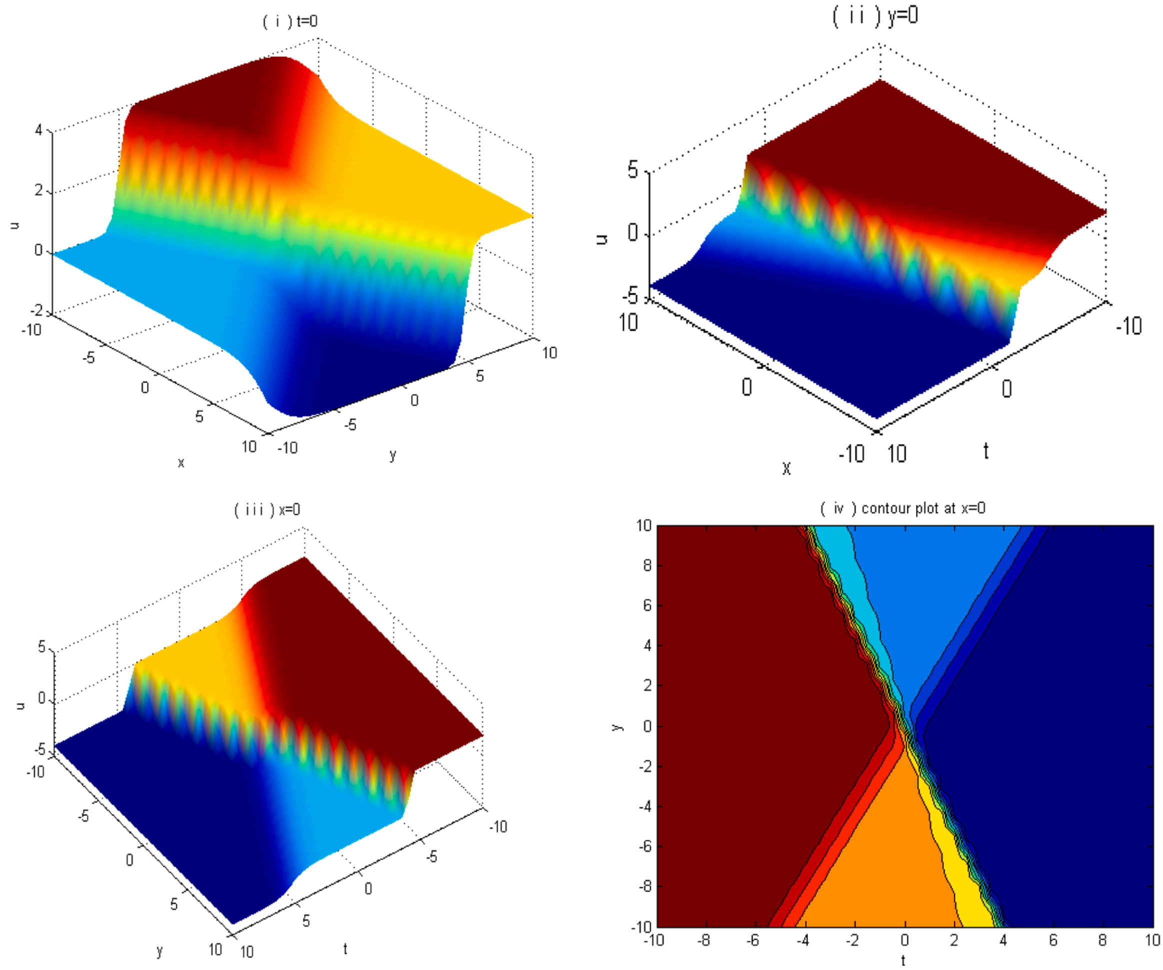

Fig. 1. Two-kink wave solution for Eq. (9) via Eq. (1) by considering the proper parameters: $\varepsilon = 0, \eta = 1, k_1 = 1, k_2 = -2, p_1 = 1, p_2 = -2$and $\vartheta_1^0 = \vartheta_2^0 = 0$, for (i) $xy-$ plane (i) $xt-$ plane (iii) $ty-$ plane (iv) corresponding contour plot of (iii).

solution:

$$
\begin{aligned}
q_i &= \frac{-k_i^4 p_i - \eta k_i^2 p_i + 2\varepsilon}{p_i k_i^2}, (i = 1, 2), \\
C_{12} &= \frac{3k_1^4k_2^2p_1^2p_2 - 3k_1^3k_2^3p_1^2p_2 - 3k_1^3k_2^3p_1p_2^2 + 3k_1^2k_2^4p_1p_2^2 + 2\varepsilon\left(k_1^2p_1^2 - k_1k_2p_1p_2 + k_2^2p\right)_2^2}{3k_1^4k_2^2p_1^2p_2 + 3p_1^2p_2k_1^3k_2^3 + 3p_1p_2^2k_1^3k_2^3 + 3p_1k_1^2k_2^4p_2^2 + 2\varepsilon\left(k_1^2p_1^2 + k_1k_2p_1p_2 + p_2^2k_2^2\right)}.
\end{aligned}
\tag{11}
$$

Next, by substituting (9) into (5) along with (11), we obtain the two-soliton wave solution of (1). If we let$\varepsilon = 0, \eta = 1, p_1 = 1, p_2 = -2, k_1 = 1, k_2 = -2$ and $\vartheta_1^0 = \vartheta_2^0 = 0$, a two-kink wave profile is derived and presented in Fig. 1. As illustrated in Fig. 1(d), the two solitons undergo mutual interaction and cross each other, exhibiting an elastic collision. An asymptotic analysis of the solution as $t \to \pm \infty$confirms that both solitons preserve their amplitude, velocity, and overall shape after the interaction, with the only effect being a finite phase shift.

By applying the above method, Eq. (9) generates breather waves by choosing appropriate constraints. These breather waves of (1) can be derived from (11) under the following conditions:

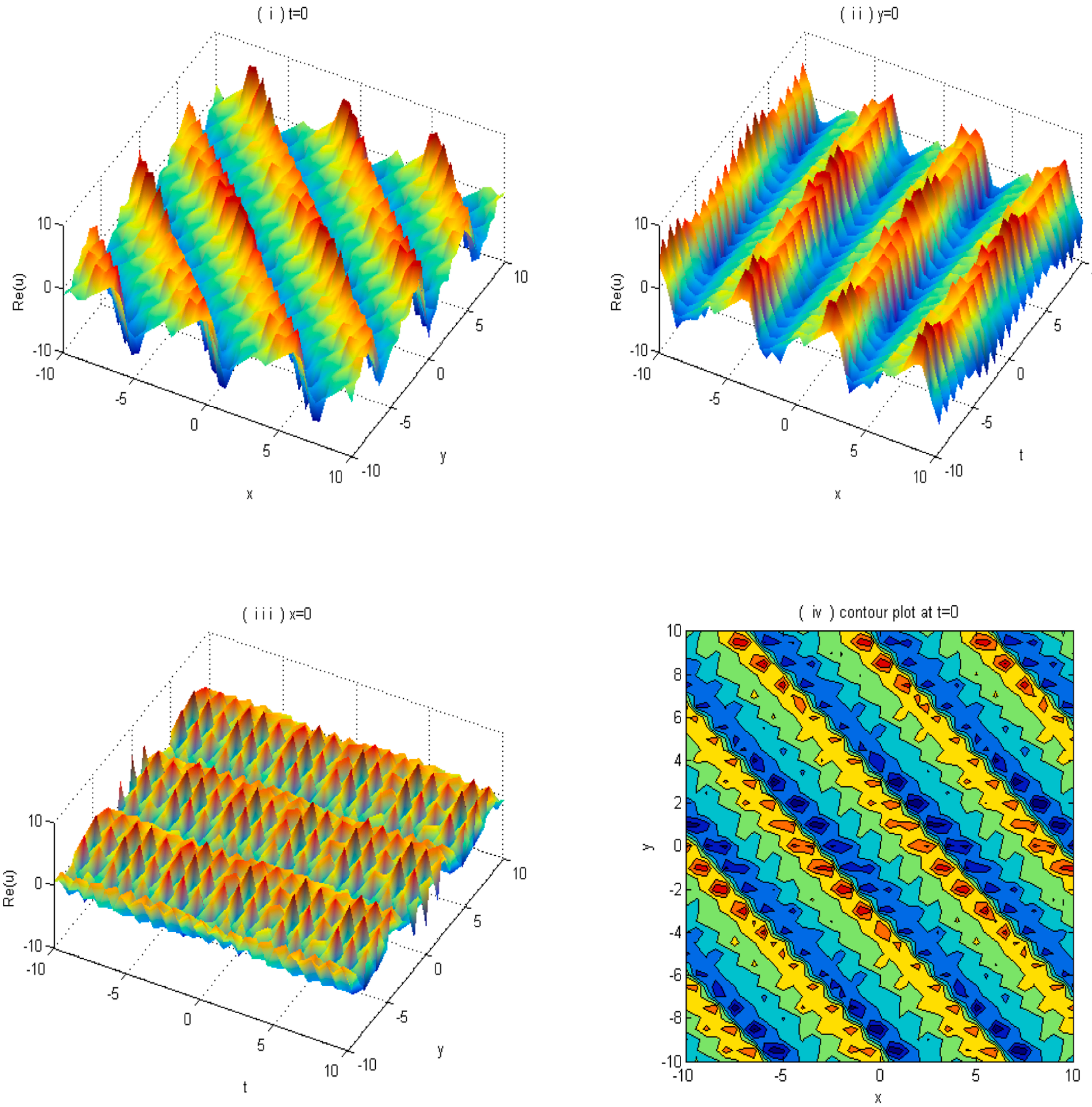

Fig. 2. Breather waves for Eq. (14) via Eq. (1) by considering the proper parameters:$\varepsilon = 0, \eta = 1, k_1 = I, k_2 = -2I, p_1 = 1, p_2 = -2,$ and $\vartheta_1^0 = \vartheta_2^0 = 0$, for (i) $xy-$ plane (i) $xt-$ plane (iii) $ty-$ plane (iv) corresponding contour plot of (i).

$$k_1 = Ib_1, k_2 = -2Ib_2, p_1 = a_1, p_2 = -2a_1, \tag{12}$$

For example, by selecting the constraints as $k_1 = I, k_2 = -2I, p_1 = 1, p_2 = -2, \vartheta_1^0 = \vartheta_2^0 = 0$, we can obtain breather solutions. Additionally, Eq. (9) can be rewritten as:

$$f = 1 + 2\cos(1.5x - 1.5y + 3t)e^{-i(0.5x-2.5y+3t)} + 1.8e^{-i(x-5y+6t)} \tag{13}$$

and thus

$$u = -\frac{2i\{e^{i(x+y)} - 2e^{-2i(x-2y+3t)} - 1.8e^{-i(x-5y+6t)}\}}{1 + 2\cos(1.5x - 1.5y + 3t)e^{-i(0.5x-2.5y+3t)} + 1.8e^{-i(x-5y+6t)}} \tag{14}$$

The waveforms derived from solution (14) display a twofold periodic structure, as shown in Fig. 2. The plots reveal different propagation behaviors depending on the plane of observation. In the $xy-$ plane, the soliton moves along a diagonal path, reflecting simultaneous evolution in both spatial directions. Conversely, in the $xt-$ and $yt-$ plane projections, the soliton propagates parallel to the $t-$ axis, indicating that it remains spatially localized while evolving over time.

However, by setting the parameters as $\varepsilon = 0, \eta = 1.25, p_1 = p_2^* = 0.5 + 2I, k_1 = 0.4, k_2 = 0.6, \vartheta_1^0 = \vartheta_2^{0*} = \pi I$, Eq. (9) reduces to:

$$\begin{aligned} f = 1 &+ e^{0.4x+0.2000y-0.5640t}e^{i\left(3.1416+0.8y+4.5120\times10^{-11}t\right)} + e^{0.6x+0.3000y-0.9660t}e^{-i\left(3.1416+1.2y+1.04328\times10^{-10}t\right)} \\ &+(0.4146341463 - 0.4682926829i)e^{1.0x+0.500y-1.5300t}e^{-i\left(0.4y+5.9208\times10^{-11}t\right)} \end{aligned} \tag{15}$$

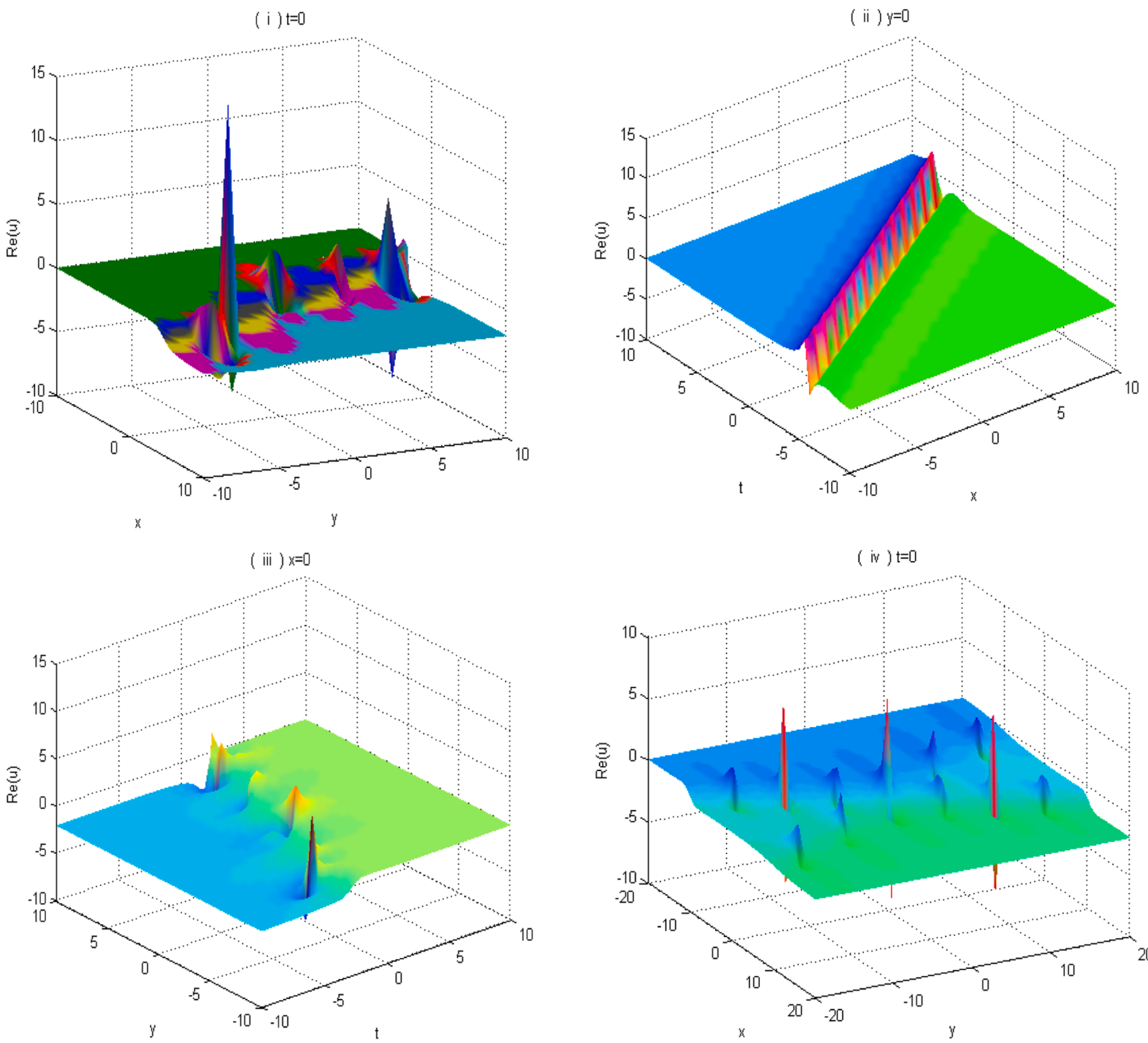

Fig. 3. Lump solutions of Eq. (1) by selecting appropriate parameters: $\varepsilon = 0, \eta = 1.25, p_1 = p_2^* = 0.5 + 2I, k_1 = 0.4, k_2 = 0.6, \vartheta_1^0 = \vartheta_2^{0*} = \pi I$, at (i) $t = 0$ (ii) $y = 0$ (iii) $x = 0$(iv) interaction of two periodic lump wave for $\varepsilon = 0, \eta = 1.25, p_1 = -p_2 = 0.5 + 2I, k_1 = 0.4, k_2 = 0.6$.

and thus

$$u = -\frac{2\left\{\begin{array}{l} 0.4e^{0.4x+0.2000y-0.5640t}e^{\alpha_1 i} + 0.6e^{0.6x+0.3000y-0.9660t}e^{-\alpha_2 i} + (0.4146341463 - 0.4682926829i) \\ e^{1.0x+0.500y-1.5300t}e^{-i\left(0.4y+5.9208\times 10^{-11}t\right)} \end{array}\right\}}{\left\{\begin{array}{l} 1 + e^{0.4x+0.2000y-0.5640t}e^{\alpha_1 i} + e^{0.6x+0.3000y-0.9660t}e^{-\alpha_2 i} + (0.4146341463 - 0.4682926829i) \\ e^{1.0x+0.500y-1.5300t}e^{-i\left(0.4y+5.9208\times 10^{-11}t\right)} \end{array}\right\}} \tag{16}$$

where, $\alpha_1 = 3.1416 + 0.8y + 4.5120 \times 10^{-11}t, \alpha_2 = 3.1416 + 1.2y + 1.04328 \times 10^{-10}t$.

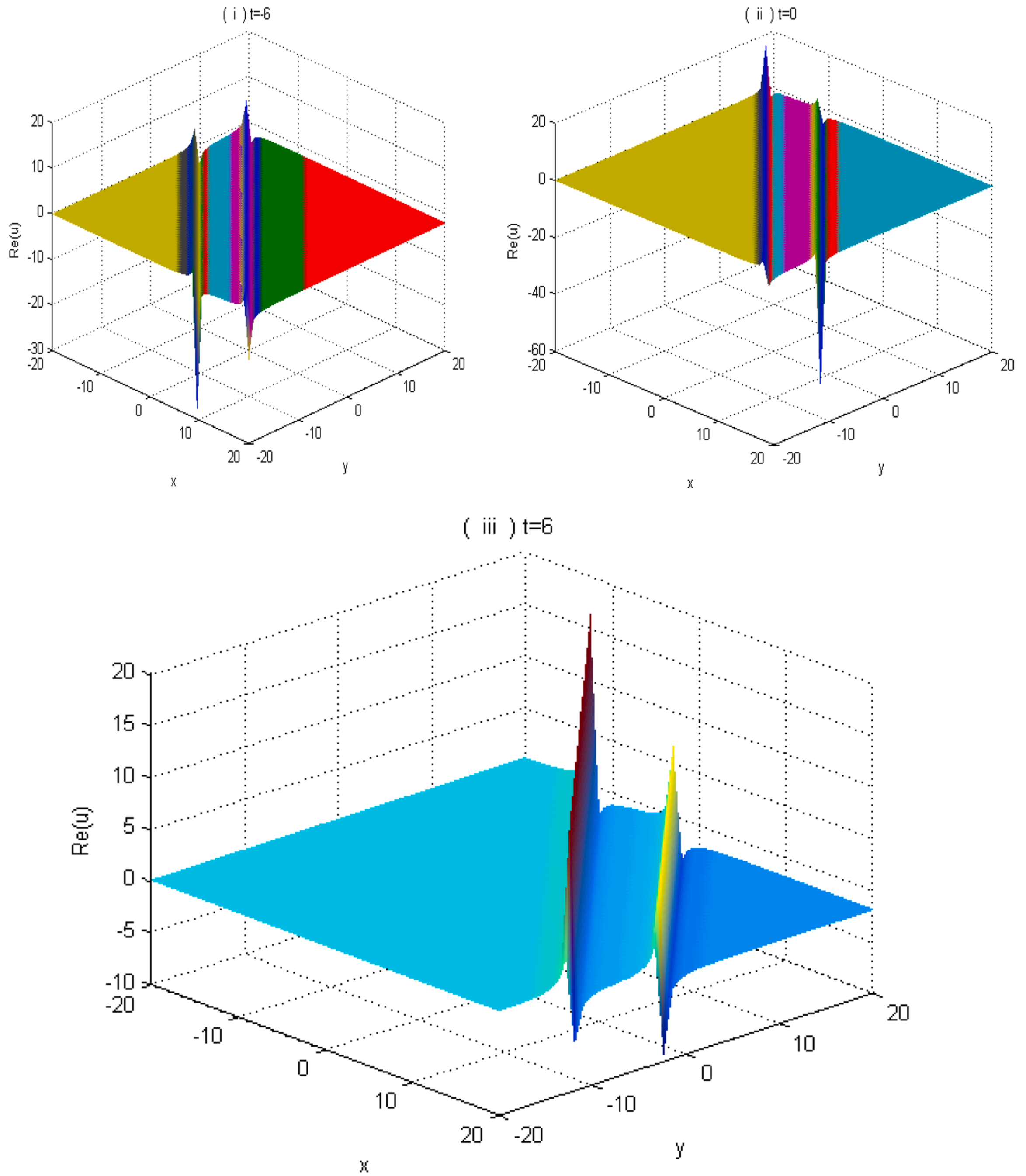

Fig. 4. Sketch of Eq. (20) by selecting appropriate parameters: $\varepsilon = 0, \eta = 1.25, p_1 = p_2 = 1, k_1 = 0.4, k_2 = 0.6, \vartheta_1^0 = \vartheta_2^{0*} = \pi I$, in $xy -$ plane at (i) $t = -6$ (ii) $t = 0$ and (iii) $t = 6$.

The solution form provided by Eq. (16) depicts periodic line lump waves, as shown in Fig. 3(i-iii).

However, by setting the parameters as $\varepsilon = 0, \eta = 1.25, p_1 = -p_2 = 0.5 + 2I, k_1 = 0.4, k_2 = 0.6, \vartheta_1^0 = \vartheta_2^{0*} = \pi I$, Eq. (9) reduces to

$$\begin{aligned} f = 1 + e^{0.4x+0.2000y-0.5640t} e^{i\left(3.1416+0.8y+4.5120\times10^{-11}t\right)} + e^{0.6x-0.3000y-0.9660t} e^{-i\left(3.1416+1.2y-1.04328\times10^{-10}t\right)} \\ + e^{1.0x-0.100y-1.5300t} e^{-i\left(0.4y+1.49448\times10^{-10}t\right)} \end{aligned} \tag{17}$$

and thus

$$u = -\frac{2\left\{0.4e^{0.4x+0.2000y-0.5640t}e^{\alpha_1 i} + 0.6e^{0.6x-0.3000y-0.9660t}e^{-\alpha_3 i} + e^{1.0x-0.100y-1.5300t}e^{-i\left(0.4y+1.49448\times10^{-10}t\right)}\right\}}{\left\{1 + e^{0.4x+0.2000y-0.5640t}e^{\alpha_1 i} + e^{0.6x-0.3000y-0.9660t}e^{-\alpha_3 i} + e^{1.0x-0.100y-1.5300t}e^{-i\left(0.4y+1.49448\times10^{-10}t\right)}\right\}} \tag{18}$$

where, $\alpha_3 = 3.1416 + 1.2y - 1.04328 \times 10^{-10}t$.

The solution pattern presented by Eq. (18) shows interaction between to periodic line lump waves, as illustrated in Fig. 3(iv).

However, by setting the parameters as $\varepsilon = 0, \eta = 1.25, p_1 = p_2 = 1, k_1 = 0.4, k_2 = 0.6, \vartheta_1^0 = \vartheta_2^{0*} = \pi I$, Eq. (9) simplifies to

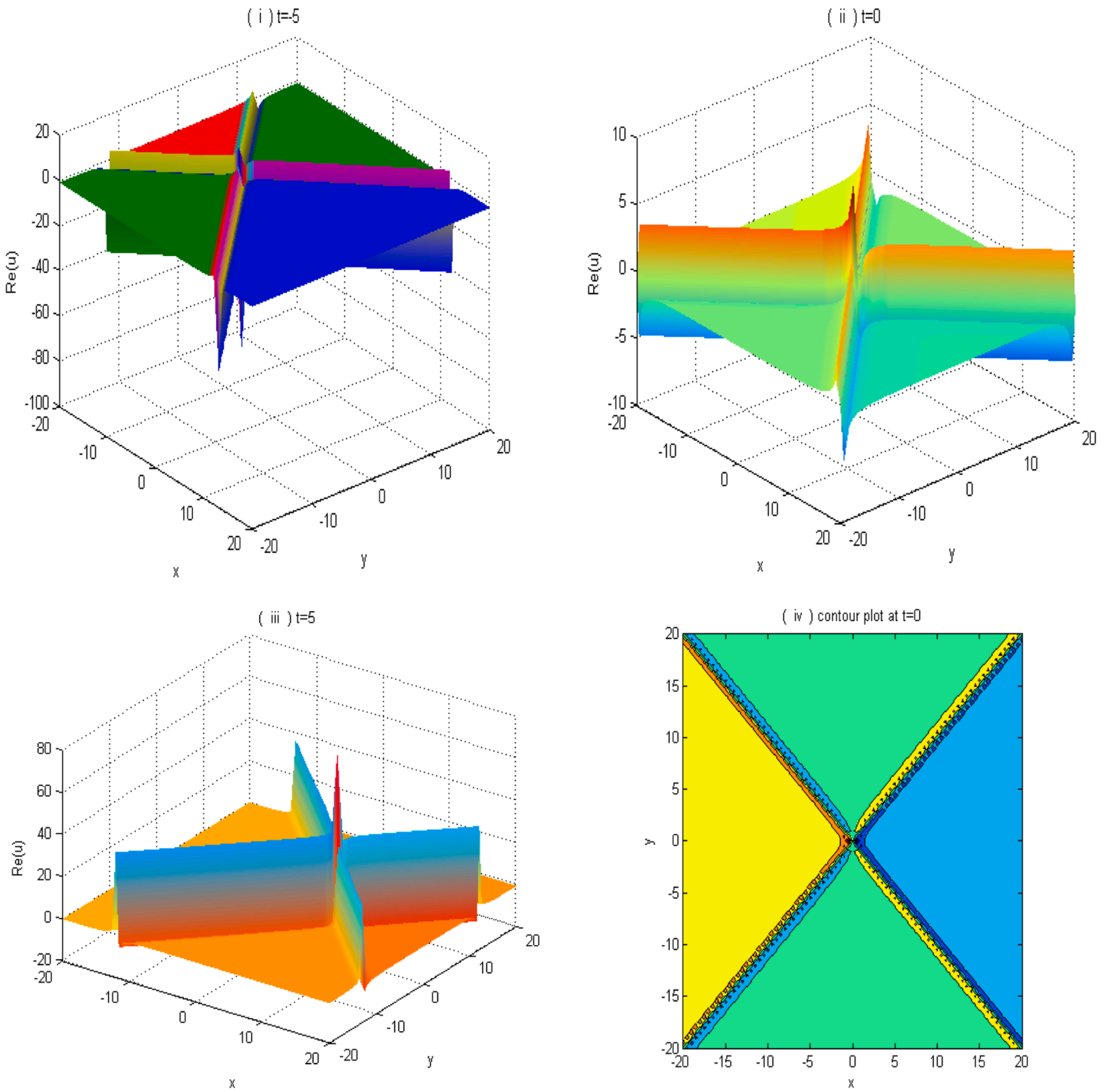

Fig. 5. Sketch of Eq. (22) by selecting appropriate parameters: $\varepsilon = 0, \eta = 1.25, p_1 = 1, p_2 = -1, k_1 = 0.4, k_2 = 0.6, \vartheta_1^0 = \vartheta_2^{0*} = \pi I$, in xy − plane at (i) $t = -5$ (ii) $t = 0$ and (iii) $t = 5$ (iv) corresponding contour plot of (ii).

$$f = 1 + e^{0.4x+0.4y-0.5640t}e^{3.1416i} + e^{0.6x+0.6y-0.9660t}e^{-3.1416i} + 0.04e^{1.0x+1.0y-1.5300t} \tag{19}$$

and thus

$$u = -\frac{2\{0.4e^{0.4x+0.4y-0.5640t}e^{3.1416i} + 0.6e^{0.6x+0.6y-0.9660t}e^{-3.1416i} + 0.04e^{1.0x+1.0y-1.5300t}\}}{\{1 + e^{0.4x+0.4y-0.5640t}e^{3.1416i} + e^{0.6x+0.6y-0.9660t}e^{-3.1416i} + 0.04e^{1.0x+1.0y-1.5300t}\}} \tag{20}$$

The solution profile provided by Eq. (20) illustrates rogue waves, as shown in Fig. 4. However, by setting the parameters as $\varepsilon = 0, \eta = 1.25, p_1 = 1, p_2 = -1, k_1 = 0.4, k_2 = 0.6, \vartheta_1^0 = \vartheta_2^{0*} = \pi I$, Eq. (9) simplifies to

$$f = 1 + e^{0.4x+0.4y-0.5640t}e^{3.1416i} + e^{0.6x-0.6y-0.9660t}e^{-3.1416i} + e^{1.0x+0.2y-1.5300t} \tag{21}$$

and thus

$$u = -\frac{2\{0.4e^{0.4x+0.4y-0.5640t}e^{3.1416i} + 0.6e^{0.6x-0.6y-0.9660t}e^{-3.1416i} + e^{1.0x+0.2y-1.5300t}\}}{\{1 + e^{0.4x+0.4y-0.5640t}e^{3.1416i} + e^{0.6x-0.6y-0.9660t}e^{-3.1416i} + e^{1.0x+0.2y-1.5300t}\}} \tag{22}$$

The solution pattern given by Eq. (22) shows periodic line lump waves, as displayed in Fig. 5. Figs. 4 and 5 illustrate the formation of distinct rogue wave patterns depending on the choice of parameters. When the parameters p_1 and p_2 are real and equal ($p_1 = p_2$), the solution yields a general rogue wave structure, characterized by a single, localized peak with a maximum amplitude at the origin.

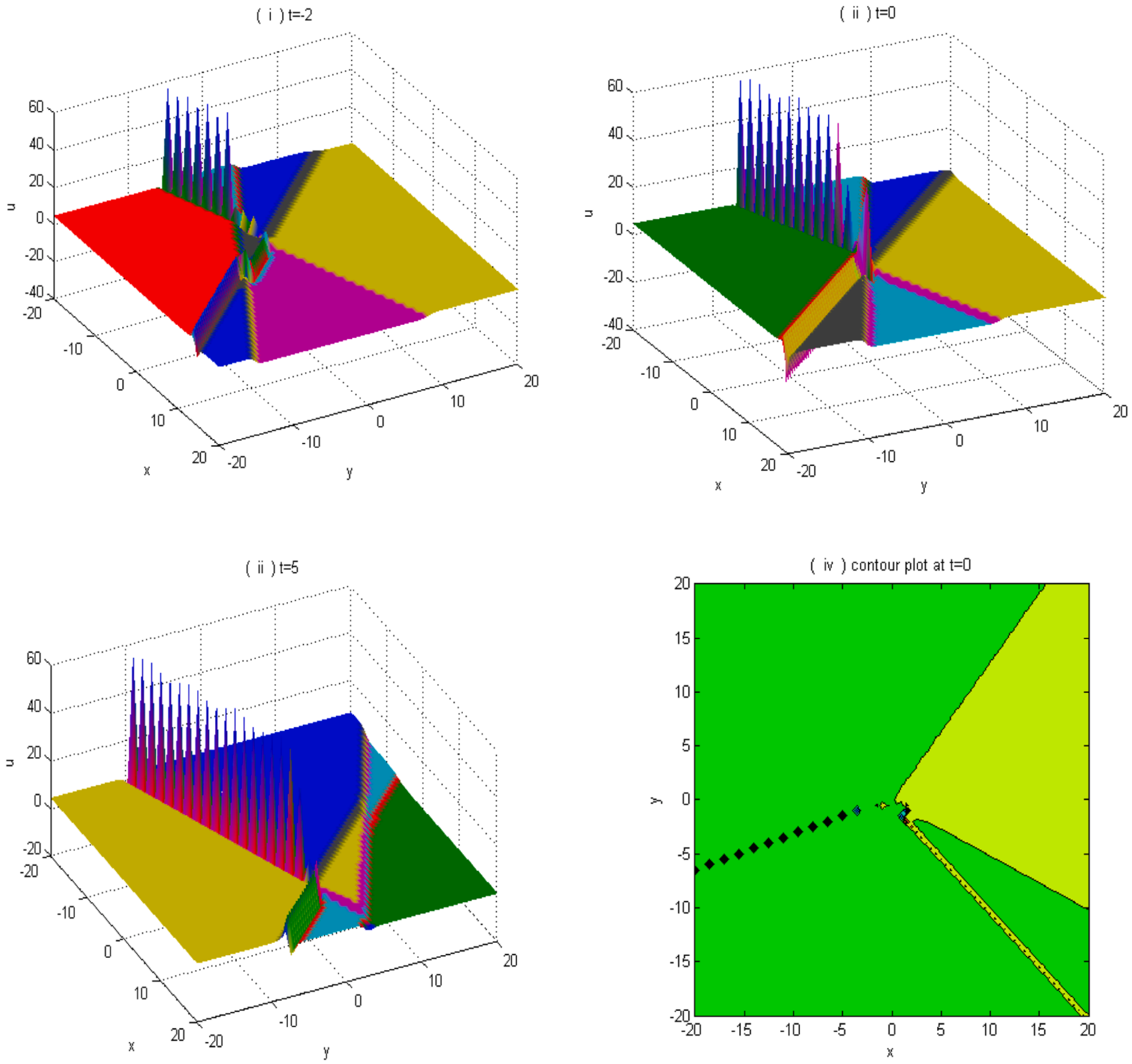

Fig. 6. The 3-kink wave solution for Eq. (23) via Eq. (1) by picking felicitous parameters: $\varepsilon = 0, \eta = 1, k_1 = -1.25, k_2 = -2, k_3 = 1, p_1 = 1, p_2 = 2, p_3 = -3$ and $\vartheta_1^0 = \vartheta_2^0 = \vartheta_3^0 = 0$, at (i) $t = -2$ (ii) $t = 0$ (iii) $t = 5$ (iv) corresponding contour plot of (ii).

Mathematically, this corresponds to the constructive superposition of terms in the solution that maximize the wave amplitude at a single point.

In contrast, when p_1 and p_2 are real, equal in magnitude, but opposite in sign ($p_1 = -p_2$), the solution produces a cross-type rogue wave pattern. In this case, the interaction terms in the solution lead to two intersecting high-amplitude peaks along orthogonal directions, resulting in the characteristic "cross" shape. These results demonstrate that the shape and orientation of rogue wave structures are highly sensitive to the parameter selection, revealing the diversity of localized wave formations supported by the model.

3.2. The 3-soliton solutions and their modified structures

We set $M = 3$, then f_3 is obtained as

$$f_3 = \begin{cases} 1 + \exp\vartheta_1 + \exp\vartheta_2 + \exp\vartheta_3 + C_{12}\exp(\vartheta_1 + \vartheta_2) + C_{13}\exp(\vartheta_1 + \vartheta_3) \\ +C_{23}\exp(\vartheta_2 + \vartheta_3) + C_{12}C_{23}C_{13}\exp(\vartheta_1 + \vartheta_2 + \vartheta_3) \end{cases}, \tag{23}$$

where,

$\vartheta_i = k_i(x + p_i y + q_i t) + \vartheta_i^0, (i = 1, 2, 3)$, and q_i, C_{ij} in which $j > i$; $i, j = 1, 2, 3$ derives off (8).

For $\varepsilon = 0, \eta = 1, k_1 = -1.25, k_2 = -2, k_3 = 1, p_1 = 1, p_2 = 2, p_3 = -3$ and $\vartheta_1^0 = \vartheta_2^0 = \vartheta_3^0 = 0$, as shown in Fig. 6, three bell-shaped solitons undergo collision, which is observed to be inelastic; that is, the soliton velocity, amplitude, and waveform are altered after interaction. Three bell-shaped solitons interact, which unite at the point $(0, 0)$, is ostensible in this image.

4. Mathematical analysis of gHSI Model

To solve Eq. (2), the equation must initially be restated in the Hirota bilinear form shown underneath

$$\left(D_x^3 D_t - D_y^2 + D_x^2 + D_y D_t + D_x D_t - D_x D_y\right)\Theta \cdot \Theta = 0, \tag{24}$$

where the bilinear differential operator from Equation (4) is adopted.

Let's now implement the subsequent transformation.

$$u = 2(\ln\Theta)_x = 2\frac{\Theta_x}{\Theta}. \tag{25}$$

Applying the operator defined in Eq. (4) to the components of Eq. (24) results in

$$\begin{aligned} &(D_x^3 D_t)\Theta \cdot \Theta = 2\Theta\Theta_{3xt} - 6\Theta_{2xt}\Theta_x + 6\Theta_{xt}\Theta_{2x} - 2\Theta_{3x}\Theta_t \\ &(D_y D_t)\Theta \cdot \Theta = 2\Theta\Theta_{yt} - 2\Theta_y\Theta_t \\ &(D_x D_y)\Theta \cdot \Theta = 2\Theta\Theta_{xy} - 2\Theta_x\Theta_y \\ &(D_x D_t)\Theta \cdot \Theta = 2\Theta\Theta_{xt} - 2\Theta_x\Theta_t \\ &(D_x^2)\Theta \cdot \Theta = 2\Theta\Theta_{2x} - 2\Theta_x^2 \\ &\left(D_y^2\right)\Theta \cdot \Theta = 2\Theta\Theta_{2y} - 2\Theta_y^2 \end{aligned} \tag{26}$$

Thus, by considering the bilinear differential operator (26) for Eq. (2) and applying the transformation (25), we obtain:

$$\begin{aligned} &2(\Theta\Theta_{3xt} - 3\Theta_{2xt}\Theta_x + 3\Theta_{xt}\Theta_{2x} - \Theta_{3x}\Theta_t) + 2\left(\Theta\Theta_{yt} - \Theta_y\Theta_t + \Theta\Theta_{xy} - \Theta_x\Theta_y + \Theta\Theta_{xt} - \Theta_x\Theta_t\right) \\ &+2\left(\Theta\Theta_{2y} - \Theta_y^2 + \Theta\Theta_{2x} - \Theta_x^2\right) = 0 \end{aligned} \tag{27}$$

Eq. (27) serves as the foundational basis upon which we will build our analytical solutions in this paper.

5. Multi-wave solutions of gHSI model

5.1. The 2-soliton solutions and their modified structures

We set $M = 2$ in Eq. (8), f_2 is obtained as

$$f_2 = 1 + \exp\vartheta_1 + \exp\vartheta_2 + C_{12}\exp(\vartheta_1 + \vartheta_2), \tag{28}$$

where,

$$\vartheta_i = k_i(x + p_i y + q_i t) + \vartheta_i^0, \tag{29}$$

By substituting (28) into (24) and simplifying, setting exponential terms' coefficients to all equal zero, getting the ensuing solution:

$$q_i = \frac{p_i^2 + p_i - 1}{k_i^2 + p_i + 1}, (i = 1, 2),$$
$$C_{12} = \frac{\xi_3 k_1^4 - 3k_2\xi_3 k_1^3 + \xi_2 k_1^2 + \xi_1 k_2^4 - 3(\xi_1 k_2^2 + \xi_5)k_1 k_2 + \xi_4 k_2^2 - (p_1 - p_2)^2}{\xi_3 k_1^4 + 3k_2\xi_3 k_1^3 + \xi_2 k_1^2 + \xi_1 k_2^4 + 3(\xi_1 k_2^2 + \xi_5)k_1 k_2 + \xi_4 k_2^2 - (p_1 - p_2)^2}, \tag{30}$$

Where $\xi_1 = p_1^2 + p_1 - 1, \xi_2 = (3p_1^2 - 2p_1p_2 + 3p_2^2 + 2p_1 + 5p_2 - 4)k_2^2 + 3p_1^2 + 2p_1p_2 + p_2^2 - 3, \xi_3 = p_2^2 + p_2 - 1, \xi_4 = p_1^2 + (3p_2 + 2)p_1p_2 + 3p_2^2 - 3, \xi_5 = (p_2 + 1)p_1^2 + (p_2 + 2)p_1p_2 + p_2^2 - 2.$

Next, by substituting (28) into (25) along with (30), we obtain the two-soliton wave of (2). By setting$k_1 = 1, k_2 = -1.25, p_1 = 2, p_2 = -2$and $\vartheta_1^0 = \vartheta_2^0 = 0$, we can derive a two-kink wave, as shown in Fig. 7.

Using the method described above, Eq. (28) generates breather waves by selecting the appropriate constraints.

These breather waves of (2) can be obtained from (30) under the following conditions:

$$k_1 = Ib_1, k_2 = -2Ib_2, p_1 = a_1, p_2 = a_1, \tag{31}$$

For example, by selecting the constraints as$k_1 = I, k_2 = -2I, p_1 = p_2 = 2, \vartheta_1^0 = \vartheta_2^0 = 0$, we can obtain breather solutions, as shown in Fig. 8. Additionally, Eq. (28) can be written as:

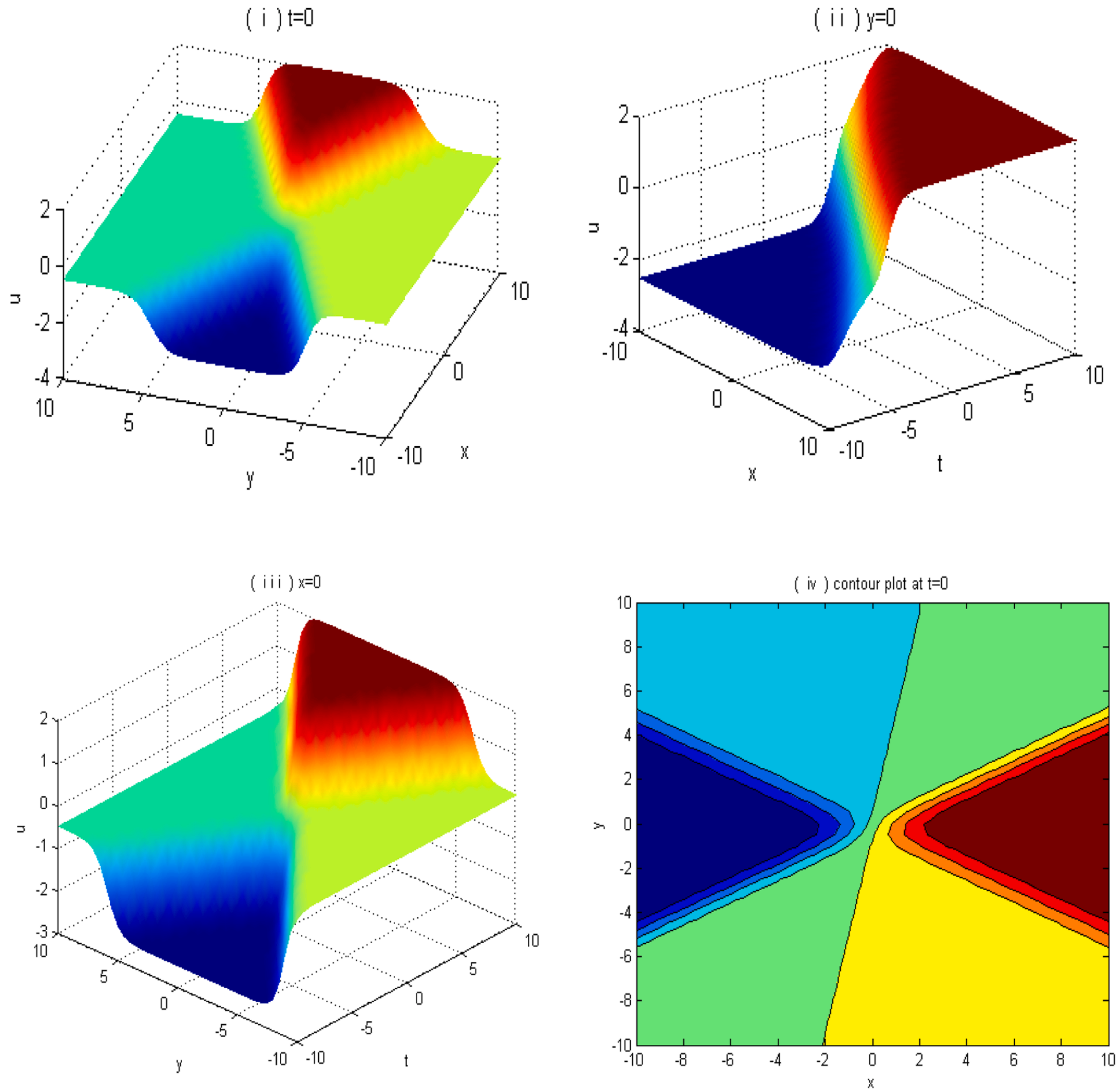

Fig. 7. The two-kink soliton solution for Eq. (28) via Eq. (2) by considering the proper parameters: $k_1 = 1, k_2 = -1.25, p_1 = 2, p_2 = -2$and $\vartheta_1^0 = \vartheta_2^0 = 0$, for (i) $xy-$ plane (ii) $xt-$ plane (iii) $ty-$ plane (iv) corresponding contour plot of (i).

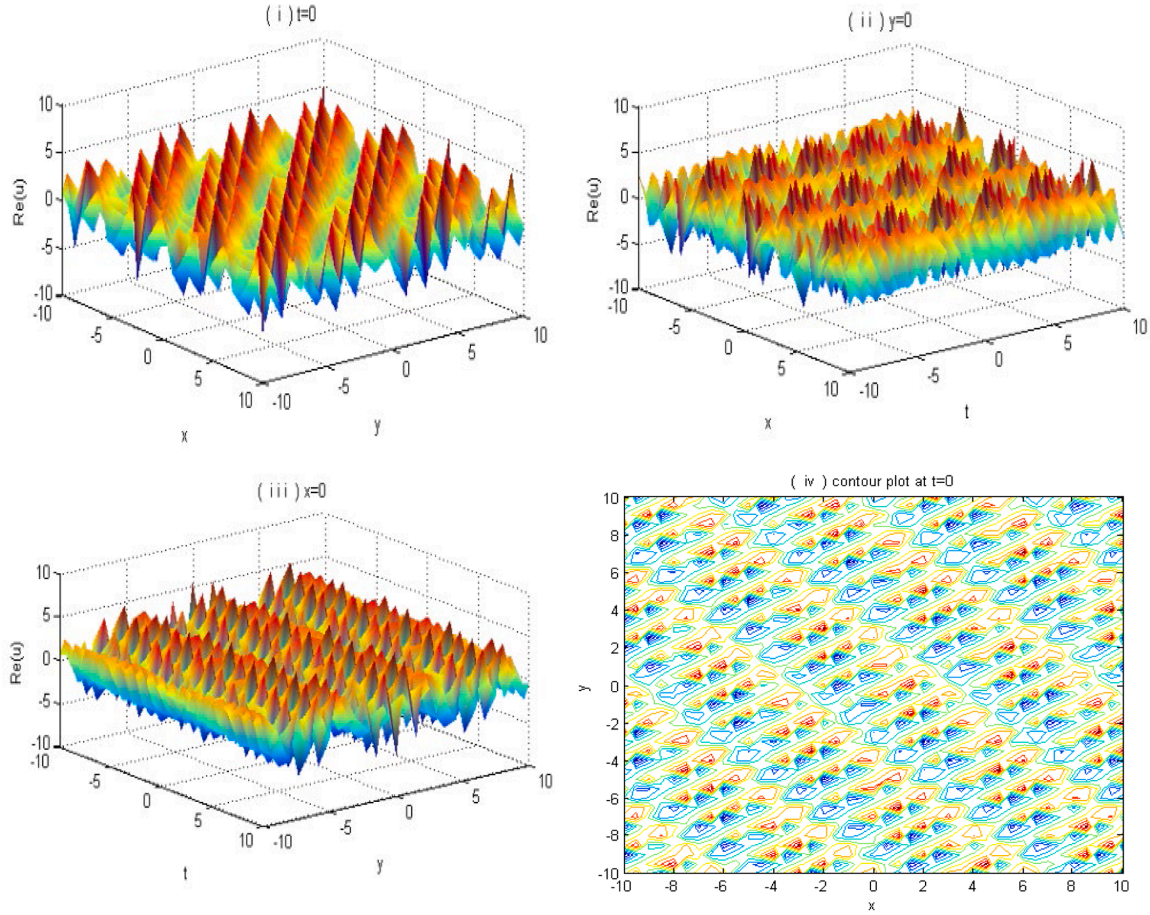

Fig. 8. Breather waves for Eq. (33) via Eq. (2) by choosing suitable parameters: $k_1 = I, k_2 = -2I, p_1 = p_2 = 2$, and $\vartheta_1^0 = \vartheta_2^0 = 0$, for (i) xy − plane (ii) xt − plane (iii) ty − plane (iv) corresponding contour plot of (i).

$$f = 1 + 2\cos(1.5x + 3y - 3.75t)e^{-i(0.5x+y-6.25t)} + 3e^{-i(x+2y-12.5t)} \tag{32}$$

and thus

$$u = -\frac{2i\{e^{i(x+2y+2.5t)} - 2e^{-2i(x+2y-5t)} - 3e^{-i(x+2y-22.5t)}\}}{\{1 + 2\cos(1.5x + 3y - 3.75t)e^{-i(0.5x+y-6.25t)} + 3e^{-i(x+2y-12.5t)}\}} \tag{33}$$

The waveforms shown in (33) display bullet-shaped, twofold periodic waves, as seen in Fig. 8.
To provide a clearer explanation for Eq. (24), a long wave limit of $f$in Eq. (28) ought to be enforced.
To do so, set the parameters as

$$k_1 = l_1\varepsilon, k_2 = l_2\varepsilon, \sigma_1^0 = \sigma_2^{0*} = I\pi, \tag{34}$$

In Eq. (28), by approaching limit as$\varepsilon \to 0$, then f may appear reformulated like:

$$f = (\theta_1\theta_2 + \theta_0)l_1l_2\varepsilon^2 + O(\varepsilon^3), \tag{35}$$

where

$$\begin{aligned} \theta_i &= x + yp_i + \left(\frac{p_i^2 + p_i - 1}{p_i + 1}\right)t, (i = 1, 2) \\ \theta_0 &= -\frac{3p_1(p_2^2 + p_1p_2 + 2p_2 + p_1) + 3(p_2^2 - 2)}{(p_1 - p_2)^2}. \end{aligned} \tag{36}$$

When Eqs. (35) and (36) are incorporated into Eq. (24), the result $u$can be shown as follows:

$$u = \frac{2(\theta_1 + \theta_2)}{(\theta_1\theta_2 + \theta_0)}. \tag{37}$$

By setting $p_i = a_i + ib_i$, two cases are obtained as follows:

Case I (Lump Solution):

For $b_i \neq 0$, the lump waves are symbolized as the associated rational solutions. Fig. 9(i) presents the dynamic behavior of the lump solutions of Eq. (37) for an appropriate choice of parameters $p_1 = 1 + 3I, p_2 = 1 - 3I$.

The lump represents a fully localized, rational solution that decays in all spatial directions while maintaining its coherent shape over time.

Case II (Rogue Wave Solution):

When $b_i = 0$, meaning p_i is a real number, we ought to depict the pattern of rogue waves using the parameters $p_1 = 0.4, p_2 = 2$, as shown in Fig. 9(ii). Clearly, Fig. 9(ii) confirms the presence of hyperbolic type rogue wave solutions.

5.2. The 3-solitons solutions and their modified structures

We set $M = 3$ in (16), so f_3 is obtained as

$$f_3 = \begin{cases} 1 + \exp\vartheta_1 + \exp\vartheta_2 + \exp\vartheta_3 + C_{12}\exp(\vartheta_1 + \vartheta_2) + C_{13}\exp(\vartheta_1 + \vartheta_3) \\ +C_{23}\exp(\vartheta_2 + \vartheta_3) + C_{12}C_{23}C_{13}\exp(\vartheta_1 + \vartheta_2 + \vartheta_3) \end{cases}, \tag{38}$$

where,

$\vartheta_i = k_i(x + p_i y + q_i t) + \vartheta_i^0, (1 \leq i \leq 3)$, and q_i, C_{ij} in which $j > i$; $i, j = 1, 2, 3$ derives off (8).

For $k_1 = 1, k_2 = 2, k_3 = 1.5, p_1 = 2, p_2 = -2, p_3 = -1$ and $\vartheta_1^0 = \vartheta_2^0 = \vartheta_3^0 = 0$, the corresponding values result in the collision of three bell solitons, as illustrated in Fig. 10. Three bell-shaped solitons interact, which converge at origin, is perceived in this image.

6. Sensitivity analysis

This section focuses on the sensitivity analysis of two models: (i) the shallow water wave (SWW) model and (ii) the generalized Hirota–Satsuma–Ito (gHSI) model. Sensitivity analysis evaluates the effect of variations in input parameters on the output of a mathematical system [41]. Identifying the parameters with the greatest influence and understanding how input variations propagate through the system is highly beneficial. Such analysis ensures that the obtained results are reliable, consistent, and robust, providing valuable guidance for decision-making in complex nonlinear systems [42].

6.1. Sensitivity analysis of shallow water wave model

To obtain the soliton solutions of Eq. (1), the following transformation relationship is considered:

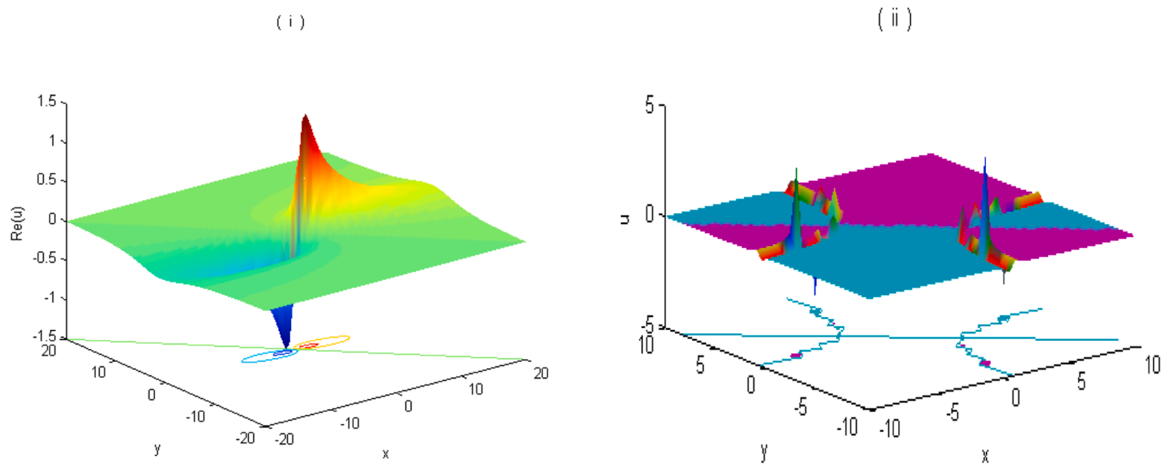

Fig. 9. (i) Lump wave of Eq. (37) for the constraints, $p_1 = 1 + 3I, p_2 = 1 - 3I$, (3D plot on top, density plot below), (ii) Rogue wave of Eq. (37) for the constraints, $p_1 = 0.4, p_2 = 2$ (3D plot on top, contour plot below).

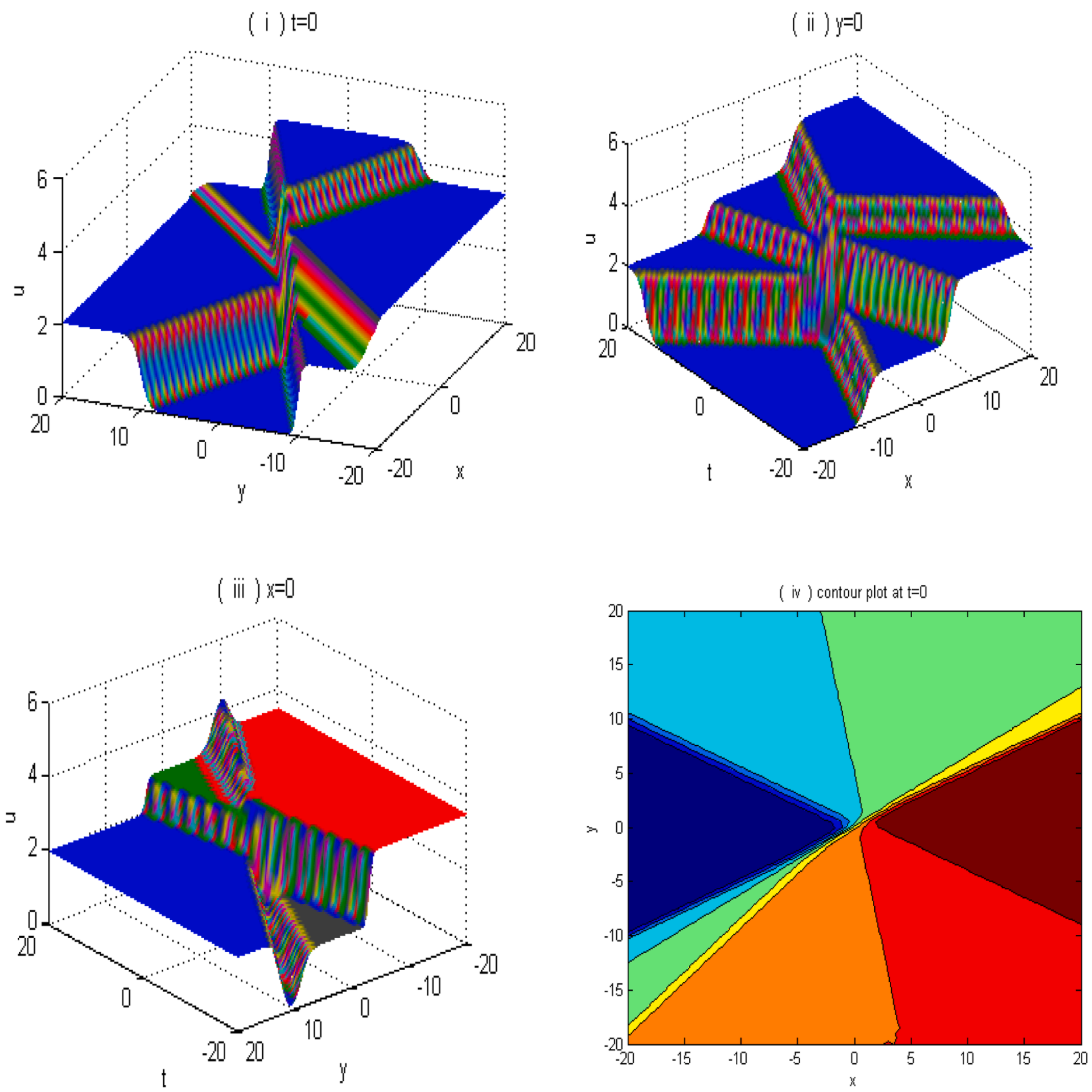

Fig. 10. The three-kink soliton solution for Eq. (38) via Eq. (2) by choosing suitable parameters: $k_1 = 1, k_2 = 2, k_3 = 1.5, p_1 = 2, p_2 = -2, p_3 = -1$ and $\vartheta_1^0 = \vartheta_2^0 = \vartheta_3^0 = 0$, for (i) $xy-$ plane (ii) $xt-$ plane (iii) $ty-$ plane (iv) corresponding contour plot of (i).

$$u(x, y, t) = u(\varsigma), \tag{39}$$

here, u represents the soliton amplitude, and $\varsigma = ax + by - ct$ denotes a soliton traveling with speed c. Based on Eq. (1) and Eq. (39), the corresponding expressions are derived,

$$3a^3bu^{iv} - 6a^2bu'u'' + (\eta ab - bc)u'' = 0 \tag{40}$$

Integrating Eq. (40) with respect to ς and the following form obtained,

$$3a^3bu''' - 3a^2b(u')^2 + (\eta ab - bc)u' = 0, \tag{41}$$

To begin this examination, here we assume $\frac{du}{d\varsigma} = v, \frac{dv}{d\varsigma} = W$, then the dynamic system is:

$$\frac{dW}{d\varsigma} = Lv^2 + Mv + \sigma\cos(\omega\varsigma), \tag{43}$$

where, $L = \frac{1}{a}$ and $M = \frac{c - \eta a}{3a^3}$ with $a \neq 0$. In Eq. (43), $\sigma\cos(\omega\varsigma)$ represents an external forcing term, where σ and ω denote the intensity and frequency of the perturbation, respectively. This section investigates the effect of initial conditions on the disturbed solution of Eq. (43) under varying intensities and frequencies, while keeping all other parameters fixed $(a = 4, c = -1, \eta = 2, \omega = 4)$. The resulting time series for the initial conditions $(-1.2, 0)$, $(-1.3, 0)$ and $(-1.4, 0)$ are illustrated in Fig. 11(a)–11(c) by the red, green, and blue curves, respectively. As shown in Fig. 11(a), when the distribution intensity is absent $(\sigma = 0)$, the periodic behavior of the disturbed structure is dependent on the initial condition. In Fig. 11(b), under low distribution intensity $(\sigma = 0.2)$, the time series curves exhibit only minor differences, indicating low sensitivity to the initial state. However, as the perturbation intensity increases $(\sigma = 1.2)$, Fig. 11(c) shows pronounced variations among the time series, highlighting a high sensitivity to changes in the initial conditions.

6.2. Sensitivity analysis of generalized Hirota-Satsuma-Ito model

According to Eq. (2) and Eq. (39), we obtain,

$$-a^3cu^{iv} - 6a^2cu'u'' + (a^2 - bc - ab - ac - b^2)u'' = 0 \tag{44}$$

Integrating Eq. (44) with respect to ς and the following form obtained,

$$-a^3cu''' - 3a^2c(u')^2 + (a^2 - bc - ab - ac - b^2)u' = 0 \tag{45}$$

To begin this examination, here we assume $\frac{du}{d\varsigma} = v, \frac{dv}{d\varsigma} = W,$ then the dynamic system is:

$$\frac{dW}{d\varsigma} = Pv^2 + Qv + \sigma\cos(\omega\varsigma), \tag{46}$$

where, $P = -\frac{3}{a}$ and $Q = \frac{a^2-bc-ab-ac-b^2}{a^3c}$with $a, c \neq 0$. In Eq. (45), $\sigma\cos(\omega\varsigma)$ represents an external forcing term, where σ and ω denote the intensity and frequency of the perturbation, respectively. This section investigates the effect of initial conditions on the disturbed solution of Eq. (45) under varying intensities and frequencies, while keeping all other parameters fixed $(a = 4, b = 2, c = -1)$. The resulting time series for the initial conditions $(-1.2, 0)$, $(-1.3, 0)$ and $(-1.4, 0)$ are illustrated in Fig. 12(a)–12(c) by the red, green, and blue curves, respectively. As shown in Fig. 12(a), when the distribution intensity is absent $(\sigma = 0$ and $\omega = 4)$, the periodic behavior of the disturbed structure is dependent on the initial condition. In Fig. 12(b), under low distribution intensity $(\sigma = 0.15$and $\omega = 4)$, the time series curves exhibit only minor differences, indicating low sensitivity to the initial state. However, as the perturbation intensity increases $(\sigma = 0.3$ and $\omega = 4.5)$, Fig. 12(c) shows pronounced variations among the time series, highlighting a high sensitivity to changes in the initial conditions.

7. Comparison with published results

In this section, we compare our work with Roshid and Ma's results in [32] and Ma, Jie and Khalique's results in [33] and along with our novelties.

7.1. Comparison our results with the Roshid and Ma's results, [32]

This subsection, we present a comparison between the results generated using Hirota's bilinear approach by Roshid and Ma's, [32] and the results obtained in our investigation as follows:

7.2. Comparison our results with Ma, Jie and Khalique's results in [33]

In this subsection, we contrast the results of our investigation with those reported by Ma, Jie and Khalique's results, [33], which were produced by applying Hirota's bilinear technique as follows:

Tables 1 and 2

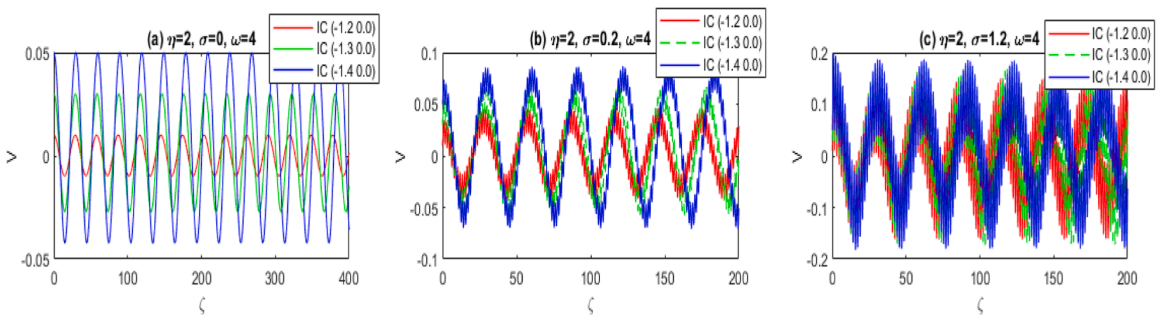

Fig. 11. Sensitivity behavior within the context of Eq. (43) (a) for $\eta = 2, \sigma = 0, \omega = 4$, (b) for $\eta = 2, \sigma = 0.2, \omega = 4$, (c) for $\eta = 2, \sigma = 1.2, \omega = 4$.

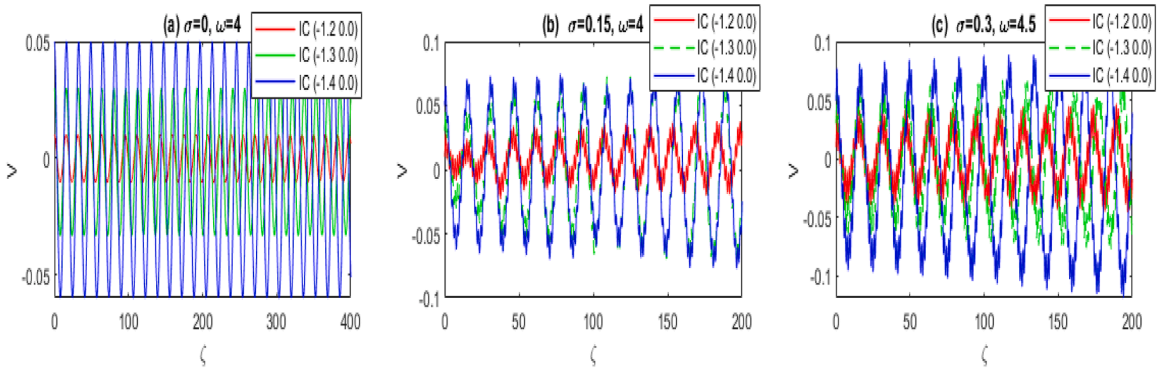

Fig. 12. Sensitivity behavior within the context of Eq. (45) (a) for $\sigma = 0, \omega = 4$, (b) for $\sigma = 0.15, \omega = 4$, (c) for $\sigma = 0.3, \omega = 4.5$.

Table 1
Comparison.

Roshid and Ma's solutions, [32]	Our research's solutions
They discussed multi-lump wave using different particular test functions, (i) $\phi = 2\sqrt{h_1}\cosh\left\{\rho_1(x+n_1y-\omega_1t)+\ln\sqrt{h_1}\right\} + h_2\sin\{\rho_2(x+n_2y-\omega_2t)\}$ (ii) $\phi = 2\sqrt{h_1}\cosh\left\{\rho_1(x+n_1y-\omega_1t)+\ln\sqrt{h_1}\right\} + h_2\cos\{\rho_2(x+n_2y-\omega_2t)\}$.	In this research, we have discussed multi-wave and multi-lump using the generalized test function $f = f_M = \sum_{\varepsilon=0,1}\exp\left(\sum_{i=1}^{M} X_i\vartheta_i + \sum_{i<j}^{M} X_iX_jC_{ij}\right)$ for $M = 2$and $M = 3$.
They failed to discuss breather wave for the SWW model.	But we have discussed breather wave for the SWW model with different structure.
There are lacks in sensitivity analysis.	We analyzed the sensitivity of this model.

Table 2
Comparison.

Ma, Jie and Khalique's solutions, [33]	Our research's solutions
They missing to discuss multi-wave for the gHSI model.	In this research, we have discussed multi-wave of gHSI mode using the test function $f = f_M = \sum_{\varepsilon=0,1}\exp\left(\sum_{i=1}^{M} X_i\vartheta_i + \sum_{i<j}^{M} X_iX_jC_{ij}\right)$ for $M = 2$and $M = 3$.
They discussed only lump solution of the gHSI.	In this research, we using long wave approach to present both lump and rogue wave for the gHSI model.
Don't discussed breather wave for the same model.	We have discussed breather wave for the same model with different structure.
There are lacks in sensitivity analysis.	We analyzed the sensitivity of this model.

7.3. Novelties in our exploration

This study applies Hirota's bilinear method to derive soliton solutions of the SWW and gHSI models in exponential function form. Both real- and complex-valued solutions are obtained, encompassing kink waves, bright–dark combinations, periodic waves, lump waves, rogue waves, double-periodic waves, and cross-lump structures. For the first time, lump and rogue wave solutions are generated using the long-wave limit approach. Furthermore, a sensitivity analysis is conducted to examine the influence of parameter variations, demonstrating the robustness, versatility, and potential applicability of the proposed models in the study of nonlinear wave dynamics.

8. Conclusion

This study presents a detailed mathematical analysis of the extended shallow water wave (SWW) and generalized Hirota–Satsuma–Ito (gHSI) models, with particular emphasis on soliton solutions. Using the Hirota bilinear method, we derived multiple soliton solutions and investigated their diverse structures, including lump and rogue wave solutions, along with a sensitivity analysis for both models. The lump and rogue wave solutions of the gHSI equation were obtained via the long-wave limit approach. The results illustrate the complex interactions among solitons and their evolution in nonlinear wave propagation. Selected results are depicted graphically to demonstrate the efficiency and effectiveness of the employed method in solving nonlinear equations. The outcomes confirm that the proposed methodology provides a clear and systematic framework for tackling a wide range of nonlinear problems through the bilinear method, which is commonly encountered in engineering and applied sciences. Building on these findings, future work will focus on examining the chaotic dynamics of the SWW and gHSI models, following the strategies outlined in [43,44].

Furthermore, the dynamical behavior of the variable-coefficient gHSI model will be explored using a similar analytical framework. This approach not only offers a robust tool for deriving exact and localized solutions but also has potential applications in modeling complex wave phenomena in fluid dynamics, plasma physics, and optical systems, thereby connecting theoretical insights with practical engineering applications.

Declaration of competing interest

The authors declare that they have no known competing financial interests or personal relationships that could have appeared to influence the work reported in this paper.

Data availability

The authors do not have permission to share data.

References

[1] Liu YH, Guo R, Zhang JW. Inverse scattering transform for the discrete nonlocal P T symmetric nonlinear schrödinger equation with nonzero boundary conditions. Phys D 2025;472(4):134528.
[2] Khater MA, Akbar MA, Akinyemi L, Inc M. Bifurcation of new optical solitary wave solutions for the nonlinear long-short wave interaction system via two improved models of expansion method. Opt Quantum Electron 2021;53:507.
[3] Liu XY, Guo R. Mixed single, double, and triple poles solutions for the space-time shifted nonlocal DNLS equation with nonzero boundary conditions via Riemann–Hilbert approach. Nucl Phys B 2024;1009(6):116742.
[4] Wang ML, Zhou YB, Li ZB. Applications of a homogeneous balance method to exact solutions of nonlinear equations in mathematical physics. Phys Lett A 1996;216:67–75.
[5] Ma WX. Soliton solutions by means of Hirota bilinear forms. Partial Differ Equ Appl Math 2022;5:100220.
[6] Kumar S, Mohan B. A novel and efficient method for obtaining Hirota's bilinear form for the nonlinear evolution equation in (n+1) dimensions, *Partial Differ*. Equ Appl Math 2022;5:100274.
[7] Hossen MB, Roshid HO, Ali MZ. Dynamical structures of exact soliton solutions to Burgers' equation via the bilinear approach. Partial Differ Equ Appl Math 2021;3:100035.
[8] Han L, Bilige S, Wang X, Li M, Zhang R. Rational wave solutions and dynamics properties of the generalized (2 + 1)-dimensional Calogero-Bogoyavlenskii-Schiff equation by using bilinear method. Adv Math Phys 2021. Article ID 9295547.
[9] Hossen MB, Roshid HO, Ali MZ, Rezazadeh H. Novel dynamical behaviors of interaction solutions of the (3 + 1)-dimensional generalized B-type Kadomtsev-Petviashvili model. Phys Scr 2021;96:125236.
[10] Liu S, Yang Z, Althobaiti A, Wang Y. Lump solution and lump-type solution to a class of water wave equation. Results Phys 2023;45:106221.
[11] Hossen MB, Roshid HO, Ali MZ. Modified double sub-equation method for finding complexiton solutions to the (1+1) dimensional nonlinear evolution equations. Int J Appl Comput Math 2017;3(3):1–19.
[12] Roshid HO. Novel solitary wave in shallow water and ion acoustic plasma waves in-terms of two nonlinear models via method. J Ocean Engin Sci 2017;2(3):196–202.
[13] Hu JY, Tian YZ, Yang YF. Optical envelope patterns in quadratic–cubic nonlinear medium by trial equation method. Optik 2021;240:166900.
[14] Yuan WX, Guo R. Physics-guided multistage neural network: A physically guided network for step initial values and dispersive shock wave phenomena. Phys Rev E 2024;110:065307.
[15] Hossen MB, Roshid HO, Ali MZ. Multi-soliton, breathers, lumps and interaction solution to the (2+1)-dimensional asymmetric Nizhnik- Novikov-Veselov equation. Heliyon 2019;5(10):e02548.
[16] Ismael HF, et al. Multiple soliton, M-lump and interaction solutions to the (3+1)-dimensional soliton equation. Results Phys 2023;45:106220.
[17] Tan W, Dai H, Dai Z, Zhong W. Emergence and space-time structure of lump solution to the (2+1)-dimensional generalized KP equation. Pramana J Phys 2017;89:77.
[18] Hoque MF, Roshid HO, Alshammari FS. Dynamical interactions between higher-order rogue waves and various forms of n-soliton solutions of the (2+1)-dimensional ANNV equation. Chin Phys B 2020;29:114701.
[19] Akhmediev N, Ankiewicz A, Taki M. Waves that appear from nowhere and disappear without a trace. Phys Lett A 2009;373:675–8.
[20] Yunfei Y, Huang L, Chen Y. N-solitons, breathers, lumps and rogue wave solutions to a (3+1)-dimensional nonlinear evolution equation. Comput Math Appl 2018;75(1):2538–48.
[21] Ma WX. Lump solutions to the Kadomtsev-Petviashvili equation. Phys Lett A 2015;379:1975–8.
[22] Cheng L, Zhang Y, Lin MJ. Lax pair and lump solutions for the (2+1)-dimensional DJKM equation associated with bilinear Bäcklund transformations. Anal Math Phys 2019;9:1741–52.
[23] Jiangen L, Yufeng Z. Construction of lump soliton and mixed lump stripe solutions of (3+1)- dimensional soliton equation. Results Phys 2018;10:94–8.
[24] Gilson CR, Nimmo JJ. Lump solutions of the BKP equation. Phys Lett A 1990;147:472–6.
[25] Yang JY, Ma WX. Lump solutions to the BKP equation by symbolic computation. Int J Mod Phys B 2016;30(1-7):1640028.
[26] Abdeljabbar A, Hossen MB, Roshid HO, Aldurayhim A. Interactions of rogue and solitary wave solutions to the (2 + 1)-D generalized Camassa–Holm–KP equation. Nonlinear Dyn 2022;110:3671–83.
[27] Imai K. Dromion and lump solutions of the Ishimori-I equation. Progr Theor Phys 1997;98:1013–23.
[28] Yong XL, Ma WX, Huang YH, Liu Y. Lump solutions to the Kadomtsev–Petviashvili I equation with a self-consistent source. Comput Math Appl 2018;75(9):3414–9.
[29] Kumar S, Mohan B, Kumar R. Lump, soliton, and interaction solutions to a generalized two-mode higher order nonlinear evolution equation in plasma physics. Nonlinear Dyn 2022;110:693–704.
[30] Yin YH, Lu X, Ma WX. Bäcklund transformation, exact solutions and diverse interaction phenomena to a (3+1)-dimensional nonlinear evolution equation. Nonlinear Dyn 2022;108:4181–94.
[31] Huang YH, Guo R. Wave breaking, dispersive shock wave, and phase shift for the defocusing complex modified KdV equation. Chaos 2024;34:103103.
[32] Roshid HO, Ma WX. Dynamics of mixed lump-solitary waves of an extended (2 + 1)-dimensional shallow water wave model. Phys Lett A 2018;382:3262–8.
[33] Ma WX, Jie Li, Khalique CM. A study on lump solutions to a generalized Hirota-Satsuma-Ito equation in (2+1)-dimensions. Hindawi 2018. Article ID 9059858, 7 pages.
[34] Karunakar P, Chakraverty S. Comparison of solutions of linear and non-linear shallow water wave equations using homotopy perturbation method. Int J Numer Methods Heat Fluid Flow 2017;27(9):2015–29.
[35] Zahran EHM, Khater MMA. Exact traveling wave solutions for the system of shallow water wave equations and modified liouville equation using extended jacobian elliptic function expansion method. Am J Comput Math 2014;4(5):455–63.

[36] Liu Y, Zhang Y, Pang J. Approximate solutions to shallow water wave equations by the homotopy perturbation method coupled with Mohand transform. FrontPhys 2023;10:1118898.
[37] Wei M, Cai J. The exact rational solutions to a shallow water wave-like equation by generalized bilinear method. J Appl Math Phys 2017;5(3):715–21.
[38] Zhang YX, Xiao LN. Breather wave and double-periodic soliton solutions for a (2+1)-dimensional generalized Hirota–Satsuma–Ito equation. Open Phys 2022;20 (1):58–65.
[39] Fan YY, Manafian J, Zia SM, Huy DTN, Le TH. Analytical treatment of the generalized Hirota–Satsuma–Ito equation arising in shallow water wave. Adv Math Phys 2021;2021. Article ID 1164838.
[40] Guo Y, Chen Y, Manafian J, Malmir S, Mahmoud KH, Alsubaie ASA. Exploring N-soliton solutions, multiple rogue wave and the linear superposition principle to the generalized Hirota–Satsuma–Ito equation. Sci Rep 2024;14:26171.
[41] Jhangeer A, Rezazadeh H, Seadawy AR. A study of travelling, periodic, quasi-periodic and chaotic structures of perturbed Fokas-Lenells model. Pramana J Phys 2021;95:41.
[42] Li Z, Hu H. Chaotic pattern, bifurcation, sensitivity and traveling wave solution of the coupled Kundu-Mukherjee-Naskar equation. Results Phys 2023;48: 106441.
[43] Gupta V, Mittal M, Mittal V. R-peak detection based chaos analysis of ECG signal. Analog Integr Circ Sig Process 2020;102:479–90.
[44] Gupta V, Mittal M, Mittal V. R-peak detection using chaos analysis in standard and real time ECG databases. IRBM 2019;40(6):341–54.